Ab initio phase diagram of oxygen adsorption on W(110)

2009 J. Phys.: Condens. Matter 21 134017

(http://iopscience.iop.org/0953-8984/21/13/134017)

J. Phys.: Condens. Matter **21** (2009) 134017 (10pp) doi:10.1088/0953-8984/21/13/134017

Ab initio phase diagram of oxygen adsorption on W(110)

M Stöhr[1], R Podloucky[1] and S Müller[2]

[1] Institute for Physical Chemistry, University of Vienna, Sensengasse 8/7, A-1090 Vienna, Austria
[2] Institute for Theoretical Physics II, University of Erlangen, Staudtstrasse 7, D-91058 Erlangen, Germany

E-mail: markus.stoehr@univie.ac.at

Received 13 October 2008, in final form 10 December 2008
Published 12 March 2009
Online at stacks.iop.org/JPhysCM/21/134017

Abstract

The phase diagram of oxygen adsorption on the W(110) surface is derived without any empirical parameters by a combination of density functional theory (DFT) calculations, the cluster expansion (CE) technique and Monte Carlo (MC) applications. Coverages up to 1 monolayer are considered corresponding to the range of oxygen concentrations, $0 \leqslant x_O \leqslant 1$. DFT results for single-site adsorption and in particular for full coverage reveal that adsorption at threefold hollow (H3) sites is by far the most stable one. Therefore, the CE is done for an atomic layer with the two H3 sublattices of the W(110) surface. Based on 60 DFT calculations with fully relaxed atomic geometries of lateral unit cells containing 12 atoms, and a ground state search for 80 394 structures, four ground state structures are found with the lateral unit cells (2×5) for $x_O = 0.20$, (2×2) (a) for $x_O = 0.25$, (2×1) for $x_O = 0.50$ and (2×2) (b) for $x_O = 0.75$. In agreement with experiments the most stable structures are (2×1) and (2×2) (b), which correspond to higher coverages. The thermodynamical stability of the two ground states at lower coverages is very weak. Detailed analysis of the relaxation of the (2×1) structure reveals sizeable lateral stresses acting on the surface tungsten atoms. On the basis of the effective cluster interactions MC simulations are performed in order to derive the critical temperatures by which the phase diagram is finally constructed.

(Some figures in this article are in colour only in the electronic version)

1. Introduction

Adsorption of oxygen on the W(110) surface has been studied in the past. Low energy electron diffraction (LEED) was used to characterize the detailed structure of the (2×1) phase [1], and the critical behavior and phase transitions at coverages of $x_O = 0.50$ [2, 3] and various other coverages [4]. (It should be noted that a coverage of $x_O = 1$ refers to the W(110) surface being completely covered with one monolayer of atomic oxygen in a (1×1) structure.) The saturated (1×1) structures were studied by Daimon *et al* [5] using full solid-angle x-ray photoelectron diffraction (XPD) and by Ynzunza *et al* [6] using solid-angle photoelectron diffraction. Ordering phenomena were investigated by Wu *et al* [7] at coverages of $x_O = 0.25, 0.50$ and 0.65. Growth kinetics was studied at the high coverage of $x_O = 0.68$ by Tringides [8]. Scanning tunneling microscopy measurements (STM) confirmed structural details [9] indicating stress effects within the adsorption structures. A number of theoretical studies were presented, which are mostly based on empirically derived parameters. To our knowledge, up to now only one density functional theory (DFT) study concerning the adsorption of single O atoms has been published [10]. In this work, interaction parameters were derived which entered a three-state lattice gas model for calculating the phase diagram. Various authors studied phase stabilities and related properties by application of a lattice gas model [11–16, 10, 17–19], in which the interaction energies are determined by fitting to experimental data: for example, Williams *et al* [13] fitted to the LEED data of Lu *et al* [11].

In the present work, for the first time we applied *ab initio* DFT techniques for studying the adsorption of atomic oxygen on W(110) for the complete coverage range $0 \leqslant x_O \leqslant 1$, and we construct the corresponding phase diagram without

any empirical parameters and ad hoc assumptions. For this purpose, the cluster expansion (CE) technique [20, 21] for the oxygen adsorbate layer was applied for which the interaction parameters were derived from a large set of DFT calculations. Finally, for determining the temperature-dependent phase stabilities Monte Carlo (MC) calculations utilizing the CE effective interaction energies were made. As a by-product, the ground state phases and their relaxed structural details with up-to-date DFT precision are available.

2. Computational aspects

The DFT calculations were performed by making use of the Vienna *ab initio* simulation package (VASP) [22, 23] within the projector augmented wave implementation for the pseudopotentials [24, 25]. The exchange–correlation functional was approximated within the generalized gradient approximation (GGA) of Perdew *et al* [26]. A plane wave basis with an energy cutoff of 400 eV was chosen. Suitable **k**-point grids were constructed according to Monkhorst and Pack [27], namely a 15 × 15 × 15 mesh for the primitive bulk unit cell and a 15 × 15 × 1 mesh for the surface slabs. For larger unit cells the **k**-point grids were scaled down accordingly. The integration over the Brillouin zone was done by the smearing method of reference [28] applying a width of 0.1 eV. The 5p semicore states of W were treated as valence states. For the geometrical relaxation the Hellman–Feynman forces were minimized with a quasi-Newton algorithm to absolute values less than 0.01 eV $Å^{-1}$. The bulk lattice constant of $a_W = 3.189$ Å corresponds to the value of our previous study [29]. For modeling, the surface asymmetric slabs with 4, 6, 7, 8, 9 and 10 layers of W and with different vacuum spacings were tested in order to determine the optimized number of layers for calculations with larger unit cells. The adsorption studies were made by constructing an asymmetric slab with 9 W layers and one oxygen layer at the top. During relaxation of the atomic positions the bottom three W layers were kept fixed. A vacuum region of ≈11 Å equivalent to 12 W(110) bulk layers was included in the unit cell. For some selected studies the *ab initio* molecular dynamics capabilities of VASP were exploited.

For the CE according to Sanchez *et al* [20] the unified cluster expansion (UNCLE) program package [30] was applied, which uses a genetic algorithm for the search of optimized structures [21]. Application of this program package to a multi-site adsorbate system was demonstrated by Lerch *et al* [31]. Because of two equivalent adsorption sites on the W(110) surface (see section 3.1 for more details) our CE was designed for these two sublattices. The total number of figures for the CE consisted of 32 pairs, 157 triplets and 34 quadruplets, for which the maximum vertex–vertex distance of the figures was 10.4 Å, 8.3 Å and 4.9 Å, respectively. For the figure selection and interaction fitting of the genetic algorithm we allowed figure sets with at least 20 and up to 45 figures, requiring a minimum of 10 pair figures within each figure set. The fitness of each figure set was determined by the cross validation score, S_{CV}. We left one structure out of the total number n of the available DFT calculated structures and used $n - 1$ DFT calculations to determine the effective cluster interactions J_F. The DFT energy E_{DFT} of the removed structure was then compared to its corresponding predicted CE energy E_{CE}. This removing procedure was repeated for each structure except those at 0 and 1 ML coverage. The cross validation score is defined by

$$S_{CV} = \sqrt{1/(n-2)\sum_{i=1}^{n-2}(E_{CE}(i) - E_{DFT}(i))^2}. \quad (1)$$

Thus, the quantity S_{CV} is not a measure of the accuracy of the fit but rather a measure of the accuracy in predicting properties for unknown structures. For the ground state search we considered all possible lateral unit cells of the W(110) surface with up to 12 W atoms, i.e. lateral unit cells of dimensions (1 × 1), (1 × 2), (1 × 3), (1 × 4), (1 × 5), (1 × 6), (1 × 7), (1 × 8), (1 × 9), (1 × 10), (1 × 11), (1 × 12), (2 × 2), (2 × 3), (2 × 4), (2 × 5), (2 × 6), (3 × 3) and (3 × 4). All these cells were constructed by corresponding multiples of the unit cell vectors a_1 and a_2, as shown in figure 2.

3. Results

3.1. Single-site adsorption

In a first step the adsorption energies of single O atoms at high-symmetry sites were calculated, which was done within a (4 × 4) unit cell. The atomic positions of O were only relaxed in the direction perpendicular to the surface (because of symmetry, lateral relaxations were forbidden). In accordance with the applied slab model the adsorption energy of atomic oxygen E_{ad} is defined by

$$E_{ad} = E_{slab} - E_{clean} - \tfrac{1}{2}E_{O_2} \quad (2)$$

in which the DFT total energies E_{slab} (slab with adsorbed oxygen), E_{clean} (clean W(110) surface) and E_{O_2} (= −9.84 eV for the free oxygen molecule) enter.

The four adsorption sites and their respective energies are shown in figure 1. The two symmetry equivalent threefold-coordinated hollow sites H3 (see also figure 2) are the most stable sites because of their lowest adsorption energy of −4.16 eV. The next lowest adsorption energy of −3.90 eV refers to the fourfold-coordinated hollow site H4. The energy difference of 0.26 eV between these two sites is not large, but adsorption at site H4 represents an unstable situation: any lateral relaxation drives the oxygen atom towards the nearest H3 sites. In other words, when an oxygen atom migrates from one site H3 to the next-nearest site H3 via site H4 it has to overcome an energy barrier of 0.26 eV. The energies of the remaining two adsorption sites are way off the value for site H3 and are therefore of no significance for ground state adsorption properties. Our results are in agreement with the study of Załuska-Kotur *et al* [10] reporting energy differences of ≈0.2 eV between sites H3 and H4, ≈1.2 eV between the H3 and the on-top site, and ≈0.8 eV between the bridge and on-top site.

At higher coverages the H3 sites remain as the most stable adsorption sites. At full (1 × 1) coverage the energy difference

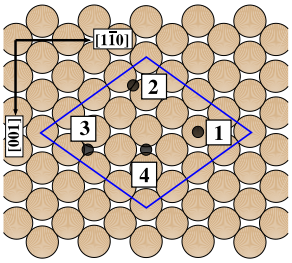

#		E_{ad} (eV)
1	ontop	-3.08
2	bridge	-3.68
3	3-site hollow (H3)	-4.16
4	4-site hollow (H4)	-3.90

Figure 1. Single-site adsorption of O on W(110): main adsorption sites and the corresponding energies of adsorption of single O (black circles) atoms on W(110). The unit cell used in the calculation is indicated in the sketch.

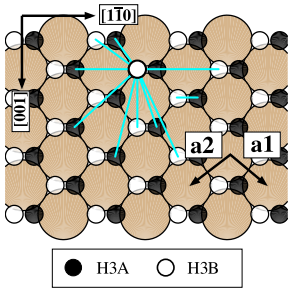

Figure 2. BCC (110) surface: threefold hollow adsorption sites as included in the multi-site cluster expansion, which is made for the two equivalent sublattices H3A (black circles) and H3B (white circles). Nearest-neighbor distances within are indicated by lines. For the construction of the set of unit cells required by the cluster expansion multiples of the primitive unit cell vectors a_1 and a_2 were used. For more details, see the text.

between H3 and H4 is strongly increased up to 0.81 eV. As a further test for finding the minimum adsorption energy we carried out molecular dynamics simulations for the coverage of $x_O = 1$. At first, a (4×4) unit cell with 16 adatoms was annealed at 2200 K and cooled down afterwards to 0 K. The final configuration for this simulation is indeed a regular (1×1) pattern with all O atoms residing on the same H3 sublattice. Based on these findings we can safely conclude that the cluster expansion in section 3.2 for only the two equivalent H3 sublattices will provide a physically meaningful description of the adsorption energetics for all coverages up to $x_O = 1$.

3.2. Cluster expansion

The CE was carried out for the two H3 sublattices, as discussed in section 3.1. Figure 2 sketches the geometrical set-up and the primitive unit cell vectors a_1 and a_2 which were used to constructed all required unit cells. Also shown are the shortest nearest-neighbor distances (blue lines). Since two sublattices are considered, the number of different distances between lattice sites is increased from 12 (in the case of one sublattice) to 44 up to a distance of $\| a_1 + 4a_2 \| = 0.5\sqrt{43}a_W$.

For a suitable thermodynamic formulation of the surface formation energy we make use of the concentration-dependent free energy corresponding to an asymmetric slab [32]. A coverage-dependent surface formation energy $E_{surf}(x_O)$ is then defined by

$$E_{surf}(x_O) = E_{slab} - x_O E_{full} - (1 - x_O)E_{clean} \qquad (3)$$

with the range of oxygen concentrations $0 \leqslant x_O \leqslant 1$. This surface formation energy expresses the stability of an ordered adsorbate structure (E_{slab}) relative to a fully covered (1×1) surface (E_{full}) and the clean W(110) surface (E_{clean}).

The CE was converged with the parameters as described in section 2. For the final fit we had to make DFT calculations for 60 ordered adsorbate structures. Because of the two H3 sublattices, structures with very short O–O distances of 1.13 Å might be constructed. This distance is much shorter than the bond length of 1.21 Å for the free oxygen molecule and therefore for a distance of 1.13 Å the neighboring oxygen atoms experience very strong repulsive interactions. For converging the corresponding DFT calculations relaxation only normal to the surface was allowed, because otherwise the closely spaced oxygen atoms would undergo strong lateral relaxations.

For the CE two different configuration spaces were considered. First, all unit cells with up to 8 atoms were constructed which allows oxygen atoms to occupy all H3 lattice sites as defined in the CE. By this choice the repulsive O–O interactions are described correctly. In a second step, the unit cell size was increased up to 12 atoms. For these larger unit cells the very short O–O distances were forbidden. In other words, if site H3 of one sublattice was occupied the corresponding nearest-neighbor H3 site of the second sublattice had to be empty.

Figure 3 shows all CE predictions for the second set of structures and the corresponding ground state line which connects the structures with lowest energy. Even forbidding structures with the very short O–O distances a sizeable number of structures with positive surface formation energies are found, in particular at larger coverages $x_O > 0.50$. Inclusion of the forbidden structures would result in even higher positive surface formation energies with values up to 3000 meV.

The converged CE for 60 calculated structures is shown in figure 4 in which DFT energies (black circles) and CE energies (red crosses) are compared. The maximum fitting error is 6.1 meV and the root mean square error (RMS) amounts to 2.1 meV. The value of the cross validation score of $S_{CV} = 3.7$ meV is slightly larger than the RMS value but still within the typical accuracy of DFT calculations. One might therefore safely conclude that the CE yields an accurate description of the input DFT energies as well as accurate energies for unknown structures (i.e. not calculated by DFT).

The most important structures for the adsorption system are the ground state structures. The ground state line for the DFT structures in figure 4 connects four ground states with concentrations $x_O = 0.20$, 0.25, 0.50 and 0.75. (The ground state line for the CE energies in figure 3 is identical with the DFT line.) Since we also allowed for the very short O–O distances as discussed above several structures included in the fit have large positive surface formation energies (up to 923 meV). For clarity we have omitted these structures and restricted the energy scale to a maximum of 100 meV.

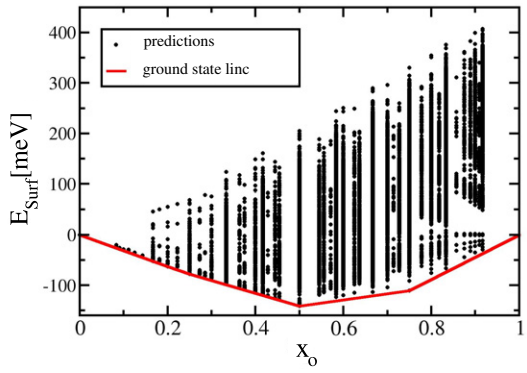

Figure 3. Concentration-dependent surface formation energy for O on W(110). Results of cluster expansion predictions for 80 394 structures as used for searching for the ground states. The ground state line (i.e. connection of structures with lowest energy) is indicated. All unit cells with up to 12 atoms are included but structures with the very short O–O distances of 1.13 Å (nearest-neighbor H3 sites) are not taken into account.

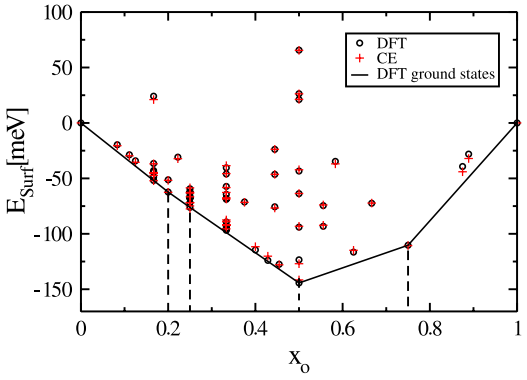

Figure 4. Comparison of density functional theory (DFT) surface formation energies and fitted cluster expansion energies (CE) for 60 ordered structures. Four ground states are detected at $x_O = 0.20$, 0.25, 0.50 and 0.75, and their energies are connected by the ground state line.

For the final fit of the interaction energies a set of 32 figures was taken into account, consisting of 10 pairs, 19 triples and 3 quadruples. Figure 5 analyzes the interaction energies for different figure sizes. In the case of pairs the figure size is the vertex to vertex distance d, whereas for three- and four-body interactions the plotted distance is the mean atomic distance within the figure. The displayed figure set represents the final optimized set due to the genetic algorithm procedure. The chosen interactions include all pair interactions up to the tenth-nearest neighbors ($\sqrt{2}a_W = 4.51$ Å) and in addition triples and quadruples of different sizes. Obviously interactions for longer pairs (maximum allowed distance was 10.45 Å) are not important, since none of these were chosen by the genetic algorithm. This fact is also reflected in the decrease of the absolute value of the interaction energy with increasing interatomic distance. In analogy to the pair figures, the interaction energies of the triples and quadruples also decrease with increasing mean atomic distance. A more detailed investigation of the interaction energies shows that the main

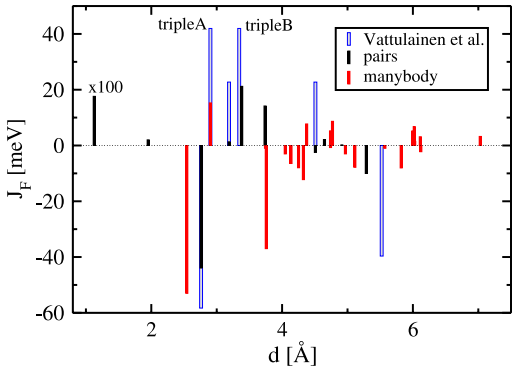

Figure 5. O adsorption on W(110): cluster interaction energies, J_F, of the cluster expansion as a function of the figure size d (for pairs: distance between the two oxygen atoms; for higher-order figures: mean distance of all positions). The set of values is divided into pair interactions and higher-order (many-body) interactions. Corresponding values of Vattulainen *et al* [15] are indicated, and two particular triple interactions (tripleA, tripleB) are marked. For further details, see the text.

contributions come from five pair interactions and three triple interactions. The main pair interactions correspond to pair distances of 1.13, 2.76, 3.38, 3.74 and 5.29 Å. For the smallest pair figure with $d = 1.13$ Å, a very large positive interaction energy of 1763 meV is obtained representing the very strong repulsion between the closely spaced oxygen atoms in the two nearest-neighbor H3 sites. The distance of 2.76 Å corresponds to the atomic spacing of the (2×1) structure along the $[1\bar{1}1]$ direction and has a sizeable attractive value of -44 meV. Figure 5 also shows the figures that were chosen by Vattulainen *et al* [15]. Their set consists of four pair interactions and two triple interactions which differ in geometry but were given the same interaction energies. Agreement with our data is only found in the case of the pair interaction at $d = 2.76$ Å, and the first triple interaction (denoted by tripleA). Models with similar interaction energies were applied by a number of authors [12, 2, 13, 10]. All these models use a smaller number of interaction energies than the one of [15].

3.3. Structures of the ground states

The atomic structures of the four ground states are sketched in figure 6. For a coverage corresponding to $x_O = 0.20$ the ground state structure is defined by a (2×5) unit cell, in which the O atoms are placed on sites of both H3 sublattices. The surface energy according to equation (3) is -62.3 meV with the minimum O–O distance of 5.52 Å. When the coverage is slightly increased to $x_O = 0.25$ the (2×2) (a) structure occurs with a surface formation energy of -76.2 meV. The minimum O–O distance is the same as for the (2×5) structure. Now the O atoms occupy only one type of H3 sublattice, as is also the case for the two ground states with higher coverages. The lowest surface energy of -144.3 meV is obtained for the (2×1) structure for a coverage of $x_O = 0.50$. There, the minimum O–O distance is reduced by a factor of 2–2.76 Å. Finally, at $x_O = 0.75$ the (2×2) (b) structure is found with a surface formation energy of -110.3 meV and also a minimum O–O distance of 2.76 Å.

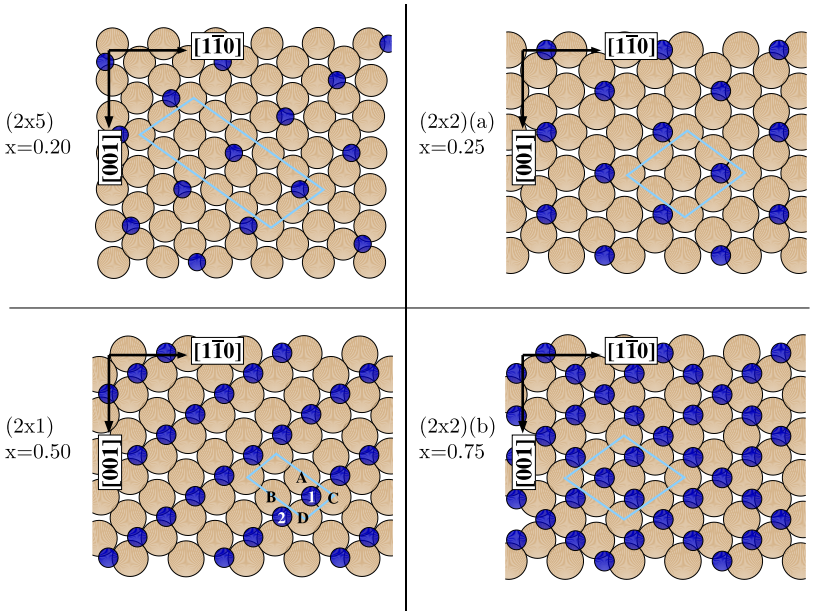

Figure 6. Atomic structure of the four ground states. The most stable structures are (2 × 1) for $x_O = 0.50$ (stabilization energy $\Delta E_{stab} = -51.1$ meV) and (2 × 2) (b) for $x_O = 0.75$ ($\Delta E_{stab} = -38.1$ meV). The low coverage structure, (2 × 5) and (2 × 2) (a), are only very weakly stable. For more details, see the text.

The thermodynamical stability at $T = 0$ K, $\Delta E_{stab}(x_O)$ of a ground state with a given concentration x_O can be defined as the difference of its surface formation energy with respect to the straight line connecting the energies of its neighboring phases. The values of ΔE_{stab} for the (2 × 5) and (2 × 2) (a) ground states are only very weakly negative, namely −1.4 meV and −0.2 meV, whereas the (2 × 1) and (2 × 2) (b) are much more stable phases with values of $\Delta E_{stab} = -51.1$ meV and −38.1 meV, respectively.

Since the absolute values for ΔE_{stab} of the (2 × 5) and (2 × 2) (a) states are very small, these states were recalculated with higher accuracy by increasing the basis size (i.e. energy cutoff up to 500 eV) and the number of **k**-points for the Brillouin zone sampling. The ground state line in figure 6 was reconfirmed, because no significant change was found in comparison to the less accurate calculations. Furthermore, the very good agreement between DFT and CE concerning surface formation energies and for finding the same ground state line strengthens the confidence in the methodology applied in our work.

Table 1 summarizes the results for the mean layer distances $\bar{d}_{i-j}$ and the layer corrugations c_i. The average height of the oxygen overlayer above the first tungsten layer is about 1.2 Å, and it is shortest for the (2 × 1) phase, namely $\bar{d}_{O-1} = 1.19$ Å. The layer distances between the first and second W layer show a direct dependence on oxygen coverage. Increasing the coverage increases also the interlayer spacing $\bar{d}_{1-2}$ from 2.19 Å for the (2 × 5) structure up to 2.25 Å for the full (1 × 1) coverage. This distance is only −0.1% smaller than the ideal bulk layer W–W distance. Layer corrugation c_i (i.e. deviation from the averaged layer distance) is also shown in table 1. Since the (2 × 2) (a), (2 × 1) and (1 × 1) structures have only one oxygen atom per primitive unit cell, there is no top layer corrugation. This restriction was lifted by performing DFT calculations for multiplies of these unit cells with reduced symmetry. However, even then no significant corrugation (<0.0005 Å) could be derived. The corrugation of the first W layer, c_1, has its maximum value of 0.13 Å for the (2 × 2) (a) structure whereas it is lowest for the (2 × 1) phase, namely 0.06 Å. The second layer corrugation, c_2, is rather constant: it takes values of 0.04–0.06 Å. For both layer relaxation as well as corrugation the values of deeper layers reach rather the bulk values of 2.25 Å and 0, respectively.

Table 1. Average layer distances $\bar{d}$ (in Å) for the adsorption ground states of O on W(110): distance $\bar{d}_{O-1}$ of O layer to surface W layer, distances $\bar{d}_{1-2}$ and $\bar{d}_{2-3}$ denote the corresponding distances of tungsten layers. Bulk layer W–W distance is 2.25 Å. Layer corrugations c_i (in Å) are also listed.

	Single	(2 × 5)	(2 × 2) (a)	(2 × 1)	(2 × 2) (b)	(1 × 1)
$\bar{d}_{O-1}$	1.23	1.22	1.21	1.19	1.20	1.21
$\bar{d}_{1-2}$	2.18	2.19	2.20	2.22	2.24	2.25
$\bar{d}_{2-3}$	2.27	2.26	2.27	2.26	2.27	2.27
c_O	—	0.00	—	—	0.03	—
c_1	0.07	0.12	0.13	0.06	0.07	—
c_2	0.02	0.05	0.05	0.04	0.06	—

Details of the atomic structures from experimental studies are only reported for the (2 × 1) [1] and (1 × 1) [5, 6] phases. For the (2 × 1) structure the reported O–W interlayer distance is 1.25 ± 0.1 Å in agreement with our findings. For the (1 × 1) structure direct evaluation of full solid-angle XPD results in an O–W interlayer distance of 1.1 Å [5] but further theoretical analysis of the same data yielded a distance of 0.84 Å. Ynzunza *et al* [6] report an interlayer distance of 0.91 Å from full solid-angle photoelectron diffraction measurements. These findings are not in agreement with our findings of 1.21 Å.

Table 2. Lateral shifts of the center of gravity for the ground state structures. The displacements $\Delta[1\bar{1}0]$ and $\Delta[001]$ (in Å) along the corresponding directions are given relative to the ideal unrelaxed structures. O: oxygen layer, 1: tungsten surface layer.

	Layer	$\Delta[1\bar{1}0]$	$\Delta[001]$
Single	O	0.088	0.000
	1	−0.001	0.000
(2 × 5)	O	0.000	0.000
	1	0.000	0.000
(2 × 2)a	O	0.027	0.000
	1	−0.003	0.000
(2 × 1)	O	0.036	−0.054
	1	−0.018	0.006
(2 × 2)b	O	0.009	0.000
	1	−0.015	0.000
(1 × 1)	O	−0.017	0.000
	1	−0.095	0.000

In our work, lateral displacements are defined by the changes of the center of mass relative to the unrelaxed structure. In general, we observe that in the presence of oxygen the first and second atomic layers of tungsten experience a net lateral shift. Table 2 lists the lateral shifts for the adsorbate oxygen and first surface tungsten layer. The displacement along the [001] direction is rather negligible with the exception of the (2 × 1) structure: the oxygen layer is shifted by −0.054 Å, whereas the tungsten surface layer is slightly shifted in the opposite direction. Along the $\Delta[1\bar{1}0]$ direction the oxygen layer experiences positive displacements for the (2 × 2) and (2 × 1) structures, and negative ones for the fully covered (1 × 1) phase. Due to symmetry, for the (2 × 5) structure no net displacement is found.

For the first W layer a clear coverage dependence is found. The higher the coverage the greater is the displacement in the $\Delta[1\bar{1}0]$ direction, and it reaches a sizeable value of −0.095 Å for the (1 × 1) phase. The second W layer (not shown) is shifted in the same direction as the first one, and the magnitude of the displacement is also increasing with coverage, but the absolute values are smaller by a factor of about ten.

For a more detailed view of the lateral displacements the individual displacements of the single atoms are sketched for the (2 × 1) structure in figure 7. As mentioned the net displacement of the first tungsten layer is in the negative $[1\bar{1}0]$ direction. This becomes clear now since the atoms labeled 'C' and 'D' are displaced by 0.043 Å and the atoms labeled 'A' and 'B' by 0.115 Å in the opposite direction. This effect widens the row with adsorbed oxygen atoms along $[1\bar{1}\bar{1}]$ and at the same time narrows the distances in the unoccupied row of W atoms. This leads to three different distances of oxygen to its neighboring W atoms. The closest distance is found from atom '1' to atom 'C' as 2.06 Å, whereas atoms 'A' with 2.07 Å and 'D' with 2.09 Å have slightly longer bond lengths. Due to symmetry the same distances are found from atom '2' to 'D', 'B' and 'C', respectively. This finding is in agreement with the finding of van Hove *et al* [1] reporting an O–W bond length of 2.08 ± 0.07 Å. For the lateral displacements of the other overlayer structures the discussed mechanism is similar.

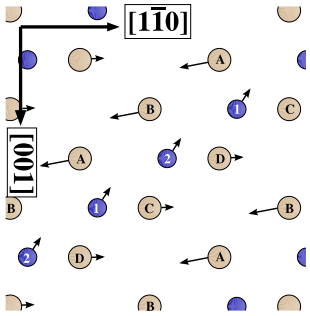

#	$\Delta[1\bar{1}0]$	$\Delta[001]$
1,2	0.036	-0.055
A,B	-0.115	0.025
C,D	0.043	-0.001

Figure 7. Lateral displacements of individual atoms of the (2 × 1) structure of O on W(110) (in Å). A, B, C, D: tungsten atoms in the surface layer; 1, 2: oxygen adlayer atoms, according to figure 6. Drawn vectors represent the displacements, the listed values of Δ represent the displacements in the $[1\bar{1}0]$ and [001] direction separately.

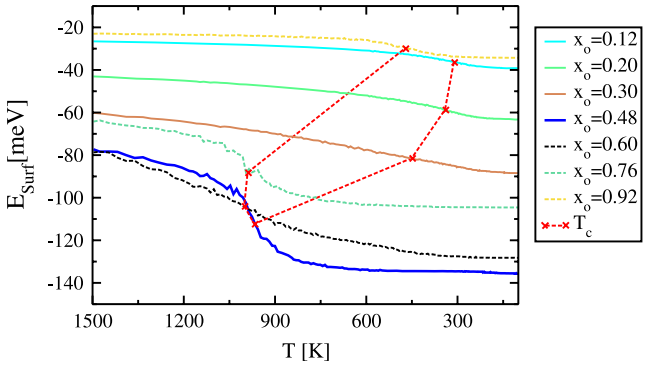

Figure 8. Monte Carlo simulation based on cluster expansion interaction energies for O on W(110). Surface energy versus temperature for various oxygen coverages for a canonical ensemble of 2 × 100 × 100 lattice sites. Critical temperature T_c (i.e. inflection points) are connected by dashed lines.

3.4. Phase diagram

Using the CE interaction energies Monte Carlo (MC) simulations for canonical ensembles were performed. The size of the simulation cell was 100 × 100 atoms, i.e. 2 × 100 × 100 lattice sites with periodic boundary conditions. Figure 8 shows the surface formation energy for various oxygen coverages versus simulation temperature. Discussing an example, for a coverage of $x_O = 0.48$, when decreasing the temperature the surface formation energy changes from ≈ -80 meV/atom to ≈ -130 meV/atom with a critical temperature of $T_c = 974$ K: at this temperature the function $E_{surf}(T)$ has an inflection point. (For an accurate determination of the critical temperature T_c the MC-derived E_{surf} was fitted to a polynomial.) We noticed that the same critical temperature is found when a fit to the temperature-dependent order parameter is done. Figure 8 also shows the energy curves for six further coverages. The qualitative shapes are similar but the curves become very flat for low and high coverages, because then the gain in ordering energy is small.

For constructing the complete phase diagram we repeated the MC procedure for 25 different coverages. The result is plotted in figure 9 in terms of a phase diagram. Up to an

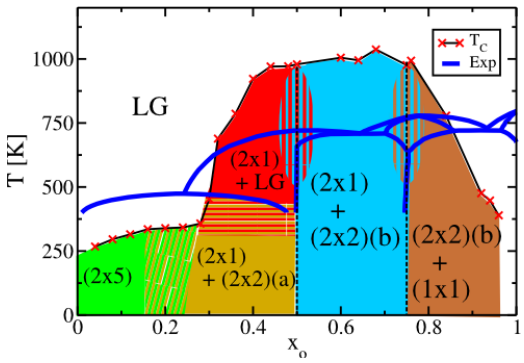

Figure 9. *Ab initio* phase diagram of O adsorption on W(110) derived from the Monte Carlo simulations as illustrated in figure 8. The actual calculated 25 points (red crosses) are connected by straight lines indicating the transition temperature T_c. Above T_c the system is in a disordered lattice-gas-like state denoted by 'LG'. Below T_c the system orders in the structures as sketched in figure 6. In some parts of the phase diagram (striped areas) a clear resolution of phases is not possible, presumably because the transition is of higher order. For more details, see the text.

oxygen coverage of $x_O = 0.28$ the critical temperature T_c is increasing slowly from 257 to 357 K. Further increasing the coverage by $x_O = 0.02$ results in a steep increase of T_c to 457 K and a further increase to 971 K at a coverage of $x_O = 0.48$. Up to a coverage of $x_O = 0.75$ the disorder–order transition temperature of 1000 K remains rather constant. For high coverages larger than $x_O = 0.75$ the critical temperature decreases linearly down to 380 K for $x_O = 0.98$.

In the ordering regime below T_c we find different mixtures of ground states. At low coverages up to $x_O = 0.16$ the ordering corresponds to the (2×5) structure. For higher coverages the (2×5) character is gradually lost and gets mixed with (2×2) (a) phases. At coverages of $x_O \approx 0.24$ small areas covered with the (2×1) structure can already be found. Up to a coverage of $x_O = 0.50$ the (2×1) structure is in coexistence with the (2×2) (a) phase at low temperatures, and at higher temperatures (above 500 K) the (2×1) phase coexists with the disordered lattice gas. The transition is found to be gradual and thus the transition region can only be sketched in an approximate way (horizontally striped area). At $x_O = 0.50$ at low temperatures a highly ordered (2×1) structure with large islands forms. Increasing the temperature decreases the island size and, consequently, the order. The predominant structure by far is the (2×1) phase, but also small areas of (2×2) (b) and disordered lattice gas can be found (vertically striped area at $x_O = 0.50$). Adding more oxygen to this phase the (2×2) (b) also appears now. As for the (2×1) case, at low temperatures the (2×1) and (2×2) (b) phases form separated areas on the surface. At a coverage of $x_O = 0.75$ the (2×2) (b) pattern appears at low temperatures. At higher temperatures (1×1) and (2×1) patches also appear (vertically striped area at $x_O = 0.75$). Finally for high coverages $x_O > 0.75$ a mixture of (2×2) (b) and (1×1) phases is found. For high temperatures the continuous areas of (2×2) (b) and (1×1) are small and grow with decreasing temperature.

On the basis of low energy electron diffraction (LEED) measurements for the full coverage range $0 \leqslant x_O \leqslant 1$ a phase diagram was first constructed by Wang *et al* [4]. This study provided the order–disorder transition temperature and the existence regions of the different ordered structures. Later on the phase diagram was refined [33, 34] by adding more complicated coexistence regions at higher temperatures. Figure 9 shows the resulting experimental phase diagram of Wu *et al* [7]. The theoretical phase diagram, to which the reader is usually referred, is based on a study of hydrogen adsorption on W(110) by means of a lattice gas Hamiltonian consisting of four pair and two triplet interactions [35]. In this study the ratios of the interaction energies were found to be similar to those given by Ching *et al* [36] for the adsorption of oxygen on W(110). In the original work of Ching the interaction energies are constructed by considering the grand potential for the known adsorption structures (1×1), (2×1) and (2×2), and by a fit to LEED data at $x_O = 0.25$, 0.50 and 0.75. Vattulainen *et al* [37, 15, 16] used this model by fitting the interaction energies in such a way that the experimental transition temperature $T_c = 710$ K at $x_O = 0.45$ according to Wang *et al* [4] is reproduced. The resulting interaction energies are shown in figure 5. Also based on the model of Ching *et al* [36] is the phase diagram constructed by Rikvold *et al* [38]. Again, the interaction energies were chosen to reproduce the known experimental data. Williams *et al* [13] designed another model, which applied four pair interactions up to the fourth-nearest-neighbor distance, requiring that the interactions for the second-and third-nearest neighbors are equal. In the next step, the interaction parameters were fitted to the data of Lu *et al* [11] at $x_O = 0.50$ and $T_c = 730$ K. Since different sets of parameters reproduce the same data, the ratio of the parameters was finally determined by requiring that the transition temperature of 480 K for $x_O = 0.25$ is also reproduced. Załuska-Kotur *et al* [10, 17–19] refined the Hamiltonian of Williams *et al* [13] by considering both threefold and also fourfold coordinated sublattice sites. The interaction energies were chosen to reproduce the properties of the original model of Williams *et al* [13]. Finally, Ertl *et al* [12] constructed a model with three pair interactions which were compared to experimental data at $x_O = 0.50$ from various authors.

Those studies, which only involved pair interactions, were not able to construct a satisfying phase diagram for the full coverage range, because without higher-order interactions the phase diagram will be symmetric with respect to $x_O = 0.50$ (see [36] and references therein). As mentioned in [36] even for a system described by only five parameters the choice of the interaction parameters is not unique. It is only possible to optimize the interactions in such a way that experimental data for a number of coverages are reproduced. The application of the CE in our work is not hampered by such limitations because input structures for the whole coverage range enter in the expansion. By such a procedure, the phase diagram for the full coverage range can be constructed purely on an *ab initio* basis.

The *ab initio* phase diagram agrees qualitatively rather well with the experimental diagram. There are, however, some significant differences: the *ab initio* critical temperature is about 150 K too low at the lower coverages and about

Table 3. Surface vibrational energies of stretching (str) and wagging (wag) modes of adsorbed oxygen for the four ground state structures of O on W(110), as derived from a high energy electron loss spectroscopy (HEELS) experiment [39] and as calculated by DFT. For some modes a range of vibrational energies as indicated by ± is possible. Also shown are the calculated zero-point vibration energies ZPE-DFT or $F_{\mathrm{vib}}(T = 0)$, and the calculated temperature-dependent free energy differences ΔF_{vib} with respect to the fully covered (1 × 1) surface. For the lowest coverage case DFT calculations were made for the (2 × 2) (a) structure, whereas the experimental values are assigned to a disordered lattice gas (LG). All values are given in meV/atom.

	LG or (2 × 2) (a)	(2 × 1)	(2 × 2) (b)	(1 × 1)
str HEELS	66	72	79	82
str DFT	60	64 ± 1.3	65 ± 2.0	68
wag HEELS	46	48	50	53
wag DFT [001]	47	48 ± 0.2	50 ± 0.3	50
wag DFT [1$\bar{1}$0]	33	52 ± 1.4	56 ± 2.9	58
ZPE-DFT	70	82	85	88
ΔF_{vib} (0 K)	−4.6	−3.3	−2.0	0
ΔF_{vib} (400 K)	−7.6	−4.8	−2.8	0
ΔF_{vib} (900 K)	−15.3	−9.2	−5.2	0

200 K too high at higher oxygen coverages. According to the discussion about the construction of the experimental phase diagram it seems reasonable to assume that the experimental diagram is of limited accuracy.

Another possible source for the systematic deviation between calculated and experimental phase boundaries might be due to surface phonons. Elbe *et al* [39] measured phonon energies for stretching and wagging modes for the disordered (LG) phase, and the (2 × 1), (2 × 2) (b) and (1 × 1) adsorption structures, as presented in table 3. For the stretching mode the vibrational energy increases from 66 meV for the lattice gas up to 82 meV for the (1 × 1) structure. The wagging mode energy is, in general, lower by about 20–30 meV and increases weakly from 46–53 meV.

For estimating the influence of surface vibrations on the surface energy stretching and wagging modes of adsorbed oxygen for the (2 × 2) (a), (2 × 1), (2 × 2) (b) and (1 × 1) structures were investigated by calculating the forces connected to suitable displacements. The corresponding results are given in table 3.

For the stretching mode, the general experimental trend of increasing vibrational energies with increasing coverage is reproduced by the DFT calculations. The absolute DFT values, however, are lower, in general. Concerning the (2 × 2) (a) structure the DFT energy of 60 meV is lower by 10% whereas the difference increases with increasing energy: for the (1 × 1) structure the DFT vibrational energy is smaller by 20% than the experimental value. The systematic underestimation of the calculated stretching energies might be due to the two-dimensional lattice parameter, which for the DFT calculation is 3.189 Å, being slightly larger than the experimental bulk lattice parameter of 3.165 Å. This difference can be attributed to the choice of a GGA exchange–correlation functional, which is known to overestimate the lattice parameters for 5d elements. On the other hand, GGA had to be chosen for a correct description of the adsorption energetics.

Wagging modes were studied by displacing oxygen atoms in the [001] and [1$\bar{1}$0] directions. In general, the agreement with experiment is very good with the exception of the [1$\bar{1}$0] vibration for the (2 × 2) (a) structure, for which DFT yields a value of 33 meV, being significantly lower than the experimental value of 46 meV assigned to the disordered LG phase (see 3). It should, however, be noted that in the experiment no ordered low coverage (2 × 2) (a) phase could be identified.

In principle, temperature-dependent vibrational free energies $F_{\mathrm{vib}}(T)$ may also be derived from DFT calculations [40], which would involve a larger number of suitably large supercell calculations for deriving phonon dispersions and the phonon density of states, from which $F_{\mathrm{vib}}(T)$ is directly determined. Considering the vibrational corrections to the surface formation energy E_{surf} of equation (3), free energy differences ΔF_{vib} are needed, for which F_{vib} for the fully covered (1 × 1) surface is the reference.

Adopting a simple model for these corrections we assume an Einstein-like model in which for each structure the phonon density of states is replaced by the three vibrational energies given in table 3. Zero-point energies in general (see also table 3) are positive values. However, the differences $\Delta F_{\mathrm{vib}}(T = 0)$ are negative, because the reference value of the (1 × 1) structure is the largest, and the lowering effect is larger the smaller the coverage is. For $T > 0$, vibrational entropies gain in influence and the described lowering effect is even more pronounced. Because of the lowering of the formation energies E_{surf} at all temperatures the ground state energies for all studied phases are also lowered correspondingly. From these considerations, one can estimate the error for not including vibrational free energies, which is at least 10 meV for temperatures $T > 400$ K, resulting in an error of the transition temperature of about 100 K. In all cases, the vibrational correction lowers E_{surf} and consequently favors the formation of ordered ground state structures at higher transition temperatures than without the corrections. Since the correction for lower coverages is larger we would expect a larger increase of T_{c} than for the higher coverages. It should, however, be noted that all arguments so far are based on only on coverage-dependent vibrational properties. In principle, temperature-dependent vibrational free energies are needed for all input structures of the CE. From such an expensive approach, temperature-dependent cluster interaction energies could be derived which would also enter the MC simulations. Such a task is certainly beyond the scope of our paper. The previously discussed semi-empirical studies are based on fitting parameters to experimental data, and therefore they implicitly comprise the influence of surface phonons. However, as pointed out before, this is probably only valid for coverages for which the corresponding models were applied. Another remarkable point of our study is, that we find a different ordering behavior at low coverages. All experimental studies report that up to a coverage of $x_{\mathrm{O}} = 0.50$ the (2 × 1) structure is the only ordered ground state, and therefore only mixtures of this (2 × 1) phase and the disordered lattice gas phase are considered. We, however, as discussed at length, confirmed two ground states for coverages of $x_{\mathrm{O}} = 0.20$

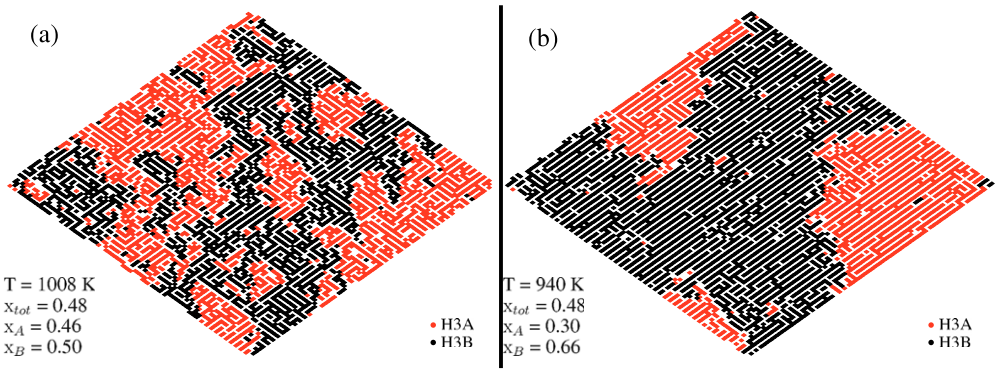

Figure 10. Distribution of oxygen on threefold hollow adsorption sites of W(110) according to the Monte Carlo simulation as based on the cluster expansion. (coverage $x_O = 0.48$, critical temperature $T_c = 974$ K). (a) For $T_c < T = 1008$ K, (b) for $T_c > T = 940$ K. Red: oxygen atoms on sublattice sites H3A; black: oxygen atoms on sites H3B; white: unoccupied sites.

and 0.25. Although their thermodynamical stability ΔE_{stab} is small, for coverages up to $x_O = 0.50$ we find regions which contain mixtures including these two phases.

For analyzing the phase stabilities in real space figure 10 shows the distribution of adsorbed oxygen atoms for $x_O = 0.48$ and temperatures above and below the critical temperature. Since the CE also takes into account the repulsive interactions, one will never find two oxygen atoms with the short distance of two nearest neighbor H3–H3 sites At $T = 1008$ K, which is slightly above $T_c = 974$ K, the tendency of ordering is only very weak. At 940 K, which is just below T_c, oxygen atoms form contiguous islands on one sublattice (either H3A or H3B) with distinctly longer ranged ordering than for $T = 1008$ K. As described above, by lowering the temperature the ordering within the island is increased, and concomitantly the contiguous areas grow. Considering figure 10, with decreasing temperature the island of oxygen atoms on the sublattice H3A will shrink and the islands of H3B sites continue to grow.

4. Summary

The aim of our work was to demonstrate the power of the combination of density functional theory calculations, the cluster expansion and Monte Carlo calculations for the truly *ab initio* derivation of the phase diagram of an adsorbate system, namely oxygen on the W(110) surface.

The results of the density functional theory approach for single-site adsorption and for full coverage reveal that the most stable adsorption site H3 is of threefold hollow geometry. On the W(110) surface two equivalent H3 sublattices exist, which have to be taken into account by a multi-site cluster expansion.

Combining density functional theory and cluster expansion four ground states of oxygen adsorbate structures were identified. The most important and stable adsorbate phases are the (2×1) and (2×2) (b) structures at higher coverages. At lower coverages the (2×5) and (2×2) (a) ground states are thermodynamically only very weakly stable and are therefore of less importance for the energetics of the adsorbate system. Indeed, in experiments only the (2×1) and (2×2) (b) structures could be identified.

We also discussed the main structural details of the ground states and showed that the center of gravity of the adlayer of oxygen and the first tungsten layer experience a significant lateral shift. The net effect is that the tungsten surface is compressed in unoccupied surface regions whereas it is expanded in regions where oxygen is adsorbed.

From Monte Carlo simulations based on the interaction energy of the cluster expansion a phase diagram emerged, which is in good agreement with experimental findings. Some systematic deviations are observed: at lower coverages ($x_O < 0.3$) the *ab initio* order–disorder transition temperature is lower by about 150 K, whereas at higher coverages ($x_O > 0.4$) the situation is reversed. A possible source of these deviations might be the neglect of surface phonons.

Because all atomistic information is available the development of ordering when cooling down from above the transition temperature to lower temperatures can be visualized by the arrangement of adsorbed oxygen atoms, forming islands of shorter or longer ranged ordered structures.

Acknowledgments

We gratefully acknowledge the support of the Austrian Science Fund (FWF) under project WK04 and Joint Research Program S90.

References

[1] Van Hove M A and Tong S Y 1975 *Phys. Rev. Lett.* **35** 1092–5
[2] Buchholz J C and Lagally M G 1975 *Phys. Rev. Lett.* **35** 442–5
[3] Baek D H, Chung J W and Han W K 1993 *Phys. Rev.* B **47** 8461–4
[4] Wang G-C, Lu T-M and Lagally M G 1978 *J. Chem. Phys.* **69** 479–89
[5] Daimon H, Ynzunza R, Palomares J, Takabi H and Fadley C S 1998 *Surf. Sci.* **408** 260–7
[6] Ynzunza R X, Palomares F J, Tober E D, Wang Z, Morais J, Denecke R, Daimon H, Chen Y, Hussain Z, Van Hove M A and Fadley C S 1999 *Surf. Sci.* **442** 27–35
[7] Wu P K, Tringides M C and Lagally M G 1989 *Phys. Rev.* B **39** 7595–610

[8] Tringides M C 1990 *Phys. Rev. Lett.* **65** 1372–5
[9] Johnson K E, Wilson R J and Chiang S 1993 *Phys. Rev. Lett.* **71** 1055–8
[10] Załuska-Kotur M A, Krukowski S, Romanowski Z and Turski Ł A 2001 *Phys. Rev.* B **65** 045404
[11] Lu T M, Wang G C and Lagally M G 1977 *Phys. Rev. Lett.* **39** 411–4
[12] Ertl G and Schillinger D 1977 *J. Chem. Phys.* **66** 2569–73
[13] Williams E D, Cunningham S L and Weinberg W H 1978 *J. Chem. Phys.* **68** 4688–93
[14] Uebing C and Gomer R 1997 *Surf. Sci.* **381** 33–48
[15] Vattulainen I, Merikoski J, Ala-Nissila T and Ying S C 1998 *Phys. Rev.* B **57** 1896–907
[16] Vattulainen I, Ying S C, Ala-Nissila T and Merikoski J 1999 *Phys. Rev.* B **59** 7697–707
[17] Załuska-Kotur M A, Krukowski S and Turski Ł A 2003 *Phys. Rev.* B **67** 155406
[18] Zaluska-Kotur M A, Lusakowski A, Krukowski S and Turski L A 2004 *Surf. Sci.* **566–568** 210–5
[19] Zaluska-Kotur M A, Krukowski S, Lusakowski A and Turski L A 2007 *Phys. Rev.* B **75** 115412
[20] Sanchez J M, Ducastelle F and Gratias D 1984 *Physica* A **128** 334–50
[21] Blum V, Hart G L W, Walorski M J and Zunger A 2005 *Phys. Rev.* B **72** 165113
[22] Kresse G and Hafner J 1993 *Phys. Rev.* B **47** 558–61
[23] Kresse G and Furthmüller J 1996 *Phys. Rev.* B **54** 11169–86
[24] Blöchl P E 1994 *Phys. Rev.* B **50** 17953–79
[25] Kresse G and Joubert D 1999 *Phys. Rev.* B **59** 1758–75
[26] Perdew J P, Burke K and Ernzerhof M 1996 *Phys. Rev. Lett.* **77** 3865–8
[27] Monkhorst H J and Pack J D 1976 *Phys. Rev.* B **13** 5188–92
[28] Methfessel M and Paxton A T 1989 *Phys. Rev.* B **40** 3616–21
[29] Stöhr M, Podloucky R, Gabl M, Memmel N and Bertel E 2007 *Phys. Rev.* B **76** 195449
[30] Lerch D, Wieckhorst O, Hart G L W, Forcade R W and Müller S *Modelling Simul. Mater. Sci. Eng.* submitted
[31] Lerch D, Wieckhorst O, Hammer L, Heinz K and Müller S 2008 *Phys. Rev.* B **78** 121405
[32] Lozovoi A Y, Alavi A and Finnis M W 2001 *Comput. Phys. Commun.* **137** 174–94
[33] Lagally M G, Lu T-M and Wang G-C 1980 *Ordering in Two Dimensions* (New York: Elsevier)
[34] Wu P K 1987 *PhD Thesis* University of Wisconsin-Madison
[35] van der Veen J F and Van Hove M A (ed) 1987 *The Structure of Surfaces II* (Berlin: Springer) p 470
[36] Ching W Y, Huber D L, Lagally M G and Wang G C 1978 *Surf. Sci.* **77** 550–60
[37] Vattulainen I, Merikoski J, Ala-Nissila T and Ying S C 1996 *Surf. Sci.* **366** L697–702
[38] Rikvold P A, Kaski K, Gunton J D and Yalabik M C 1984 *Phys. Rev.* B **29** 6285–94
[39] Elbe A, Meister G and Goldmann A 1997 *Surf. Sci.* **371** 438–44
[40] Pfeiler W (ed) 2007 *Alloy Physics* (New York: Wiley–VCH) pp 601–6